Estuarine, Coastal and Shelf Science 318 (2025) 109225

Contents lists available at ScienceDirect

Estuarine, Coastal and Shelf Science

journal homepage: www.elsevier.com/locate/ecss

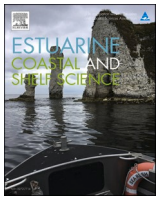

Artificial reef site-specific design under upwelling favourable winds: Ría de Ares-Betanzos (NW Iberian Peninsula)

Rodrigo Carballo [a], Iván López [a,*], David Mateo Fouz [a], María Isabel Lamas [b], Luis Carral [b]

[a] Área de Ingeniería Hidráulica, EPSE, Campus Terra, Universidade de Santiago de Compostela, 27002, Lugo, Spain
[b] Escola Politécnica de Enxeñaría de Ferrol (EPEF), Campus Industrial de Ferrol, CITENI, Universidade da Coruña, Rúa Mendizabal s/n, 15403, Ferrol, Spain

ARTICLE INFO

Keywords:
Artificial reef design
Estuaries
Galician rías
Wind-induced circulation
Numerical modelling

ABSTRACT

The placement of artificial reefs on the seafloor alters the water velocity field, promoting proper nutrient circulation and thus improving the richness of ecosystems. This nutrient circulation is closely related to water currents, which in turn can be driven or influenced by wind action. The present work addresses the influence of the wind-driven circulation on the site-specific design of artificial reefs in the Ares-Betanzos estuary (NW Iberian Peninsula). To this end, a shallow water hydrodynamic circulation model is developed to compute the circulation induced by the wind, acting in conjunction with the other relevant forcings, namely the tide, river discharges, and its mixing with shelf waters. Particular attention is paid to average and intense wind-favourable upwelling conditions. The resulting velocity design parameters are used as input for near-field hydrodynamic analysis through computational fluid dynamics modelling around the artificial reef, and assess its proper design. It is found that the influence of wind action on the artificial reef design obtained for average conditions in absence of winds is limited. However, at certain locations, it is shown that wind action may induce sufficient hydrodynamic changes to require its consideration.

1. Introduction

The indiscriminate use of natural resources, together with the increasing human population density, are affecting coastal marine ecosystems with the loss of habitats and species richness (Bracho-Villavicencio et al., 2024; Portugal et al., 2016). In this critical situation, the management of these coastal areas has become a major concern for society, prompting the development of strategies to improve the management of aquaculture and artisanal fisheries (Bacher et al., 2003).

This situation is also present along the Iberian Peninsula (Reis et al., 2021), being of special interest the Galician coast, characterized by its Rías. These coastal bodies are unique ecosystems with high biological productivity, where marine species that occupy the first links of the food chain develop, being essential for achieving high yields (González-Garcés Santiso et al., 2008). However, these areas are also in need of protection due to the intense human pressure they face such as fishing, shellfishing, urbanization of their surroundings, recreational use, and so on.

In this regard, artificial reefs (AR) can contribute to improving their management strategy (Ramos-Esplá et al., 2000). Over the last decades, a progressive knowledge of AR functioning has been accumulated primarily resulting from detailed analyses of numerous AR deployments all over the world (David da Costa et al., 2022). Thus, and despite that many issues of their performance remain poorly understood (Lima et al., 2020), a common conservation and management measure can consist in using ARs (Sánchez-Caballero et al., 2023), for which new restoration concepts must be applied based on the knowledge accumulated, and in this way give support to the large number of AR projects to be developed (Wilking et al., 2023).

AR installation affects the ecosystem in different ways, being the hydrodynamics a key aspect to understand how this modification takes place. The deployment of ARs on the seabed modifies the surrounding circulation, and could promote adequate nutrient disposal. In particular, ARs lead to the modification of the flow close to their structure generating: (i) an upwelling in the stoss side which results from the separation of the flow from the seabed being redirected upwards, and (ii) turbulence at the back area, less exposed to the currents, or back eddy. The

* Corresponding author.
E-mail address: ivan.lopez@usc.es (I. López).

https://doi.org/10.1016/j.ecss.2025.109225
Received 2 December 2024; Received in revised form 19 February 2025; Accepted 27 February 2025
Available online 27 February 2025

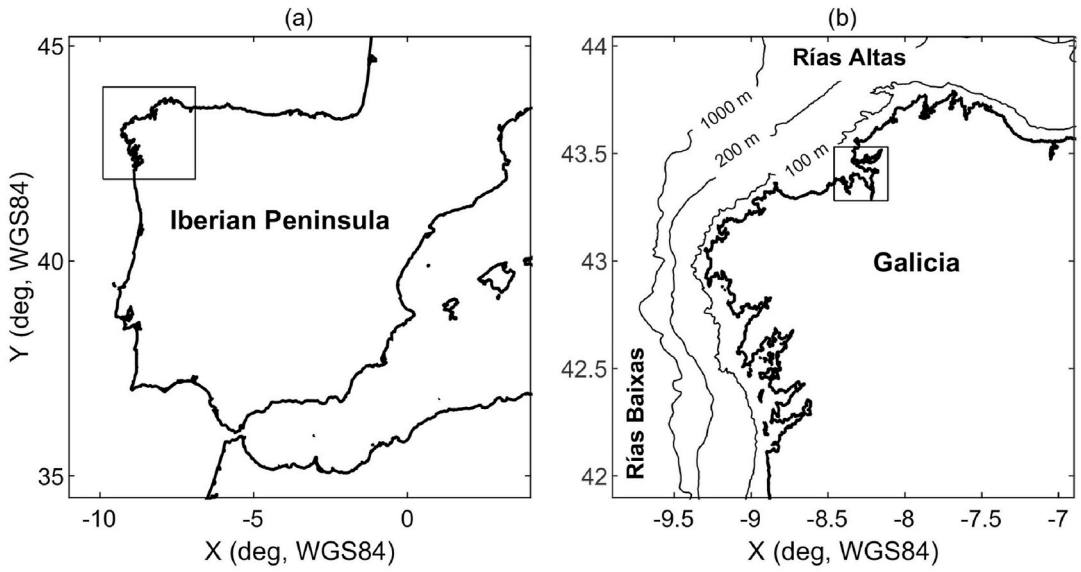

Fig. 1. – Location of the Galician Rías in the NW Iberian Península (left), which can be divided into Rías Baixas and Rías Altas (right). The area of study is indicated (right).

upwelling leads to a vertical circulation, which lifts the nutrients from the seabed transporting them through the water column, and thus its supply throughout the reef (Wang et al., 2018). In addition, this separated flow extends to the other side on the AR leading to further hydrodynamic changes which tend to accelerate seawater exchange, enhancing the overall water circulation and thus habitat conditions. Finally, the back eddy contributes to favour the circulation at the side less exposed to currents. In this area, the flow is weaker and more stable, and thus fish tend to group around it (Xue et al., 2023), and favouring the creation of nursery habitats.

In addition, after the installation of ARs at the seafloor, particulate organic matter (POM) enrichment close to the reefs is also apparent, which results from the effect of AR structures, tending to trap drifting organic material and to accumulate animals and plants that sink as they die (Falcão et al., 2009). More precisely, the term POM refers to microscopic organic water-borne particles (detritus) derived from the remains of marine organisms or introduced from land, which may exist on the seabed (Libes, 2011). Considering that the size of POM is less than 1 mm, the behaviour of these particles is considered to be determined by water flow, accumulating or dispersing along the water flow ((Kim et al., 2024). POM is a key component of the ecosystem whose presence is promoted after the installation of ARs on the seafloor ((Feng et al., 2023; Kim et al., 2024; Xu et al., 2017; Zhang, R. et al., 2021; Zhang, Z. et al., 2020)). The interaction of POM with an AR is important for preventing its sinking to the seafloor and favouring its utilisation by individuals in the ecosystem. Therefore, the hydrodynamic study of the AR seeks to understand the interaction between ARs and POM through altering the physical environment of the seafloor (Na, 2023; Xu et al., 2017), leading to high productivity (Kim et al., 2024). However, the complex interactions between ARs and POM can have both positive and negative effects on ecosystems (Kim et al., 2024), as it is the case of excessive accumulation of POM can have negative consequences, such as oxygen deficiency (Han et al., 2024; Swarzenski et al., 2008; Zhu et al., 2011).

(Kim et al., 2024)As previously stated, the appropriate functioning of an AR group is highly dependent on the surrounding hydrodynamics. Therefore, it emerges that its design should be adapted to their site-specific characteristics. To this end, an accurate hydrodynamic characterization should be conducted at the locations of interest for their deployment, and on that basis to define the most suitable AR design. In this context, one of the most promising areas for AR operation are estuaries, as it is the case of the Galician Rías (Fig. 1), a specific type of estuaries which have been previously proposed for AR deployment in the light of their high ocean productivity resulting, amongst other aspects, from their recurrent and intense upwelling events (Carral et al., 2019). In this context, it is well known that areas with recurrent upwelling and downwelling events, ascending and vortex currents, constitute appropriate sites for AR deployment (Bohnsack and Sutherland, 1985).

The Galician Rías, which can be divided into Rías Baixas (southern rias) and Rías Altas (northern rias), are mesotidal coastal areas, in many cases subject to river discharges leading to complex 3D flow patterns. Previous studies in the Galician Rías establish that the circulation in this coastal region is driven by different forcing factors, namely the tide, barotropic and baroclinic flows resulting from the presence of river discharges and oceanic water masses, along with wind action (Carballo et al., 2009; Iglesias and Carballo, 2009), with the tide being the main driving factor during average conditions. However, river inflows present different relative importance amongst Rías (Duarte et al., 2014), which in turn may significantly alter the resulting hydrodynamics, and lead to complex 3D flow patterns, even in the absence of winds.

Finally, wind induced hydrodynamics are also shown to be of great interest during specific events, in particular under intense upwelling or downwelling periods induced by the presence of high winds (Iglesias and Carballo, 2010). In the Rías Baixas, upwelling, and to a lesser extent downwelling, are recurrent events, occurring during large time periods and with high intensity, primarily resulting from their orientation (direction of their main axis) which is aligned with the predominant wind direction, i.e., N in the coastal shelf and NE in the Rías. In the case of the Rías Altas, their orientation does not correspond with that of the predominant winds leading to less intense upwelling events.

The Ría de Ares-Betanzos (Fig. 2) corresponds in a Ría Alta which has shown to be of particular interest for AR deployment, being previously proposed three specific zones (Z1, Z2 and Z3) and locations (L1, L2, and L3) to this end (Carral et al., 2019) (Fig. 2). The hydrodynamics of this Ría has been previously analysed, showing a complex 3D behaviour with river discharges leading to a positive circulation with independence of the local wind regime (Duarte et al., 2014), and with specific areas being influenced under certain conditions by the hydrodynamics of the adjacent Ría de A Coruña (to the W) and Ferrol (to the N). A more recent 3D analysis in absence of winds shows that the average circulation

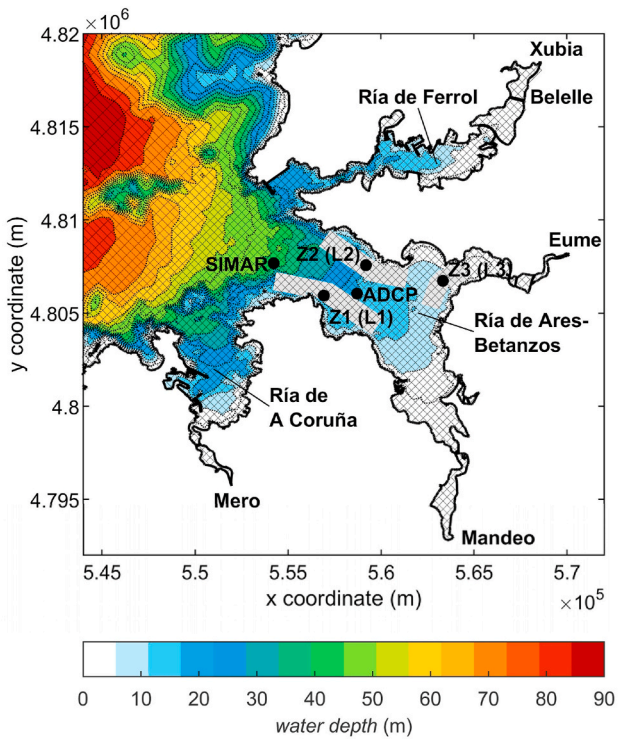

Fig. 2. – Bathymetry of the Ría de Ares-Betanzos and its surroundings, and numerical grid applied (only one in three gridlines are shown for clarity) (area indicated in Fig. 1 right). The zones of AR interest (grey areas) (Z1, Z2, Z3), and their representative locations (L1, L2, L3, respectively) are also indicated, along with SIMAR and ADCP data sites, and the main river inflows (Eume, Mandeo, Mero and Belelle).

throughout a complete average spring-neap tidal cycle does not present large variations (Carral et al., 2023a); nevertheless, the intensity of the resulting flows widely differs amongst the proposed three zones. Based on these results, i.e., average circulation in absence of wind action, preliminary AR site-specific designs were proposed.

Despite the interest of previous results, to ensure the appropriate functioning of ARs, it emerges that the influence of upwelling events on the average hydrodynamics of these zones should be also investigated. To this end, in the present work, a methodology considering seasonal wind analysis, together with 3D numerical coastal modelling (shallow water hydrodynamic circulation model), along with near-field modelling (hydrodynamic model for food delivery prediction) is applied to this coastal region to address the capability of upwelling favourable winds to alter the average circulation, and thus to adapt the available site-specific AR design in this Ría.

2. Methodology

2.1. General procedure

To assess the influence of upwelling events on the average hydrodynamics of the proposed zones and locations of interest in the Ría de Ares-Betanzos (Fig. 2), and on that basis to adapt the previous AR site-specific designs, a comprehensive methodology is proposed and applied considering different stages. This methodology is summarized in Fig. 3. Once the zones and locations of interest are identified, a thorough global and seasonal wind analysis is developed to assess the potential wind scenarios of interest with capability to alter the average circulation in absence of winds. In particular, winds generating both average upwelling and intense upwelling are investigated. To this end, the closest set of large wind data currently available is used, a SIMAR point located

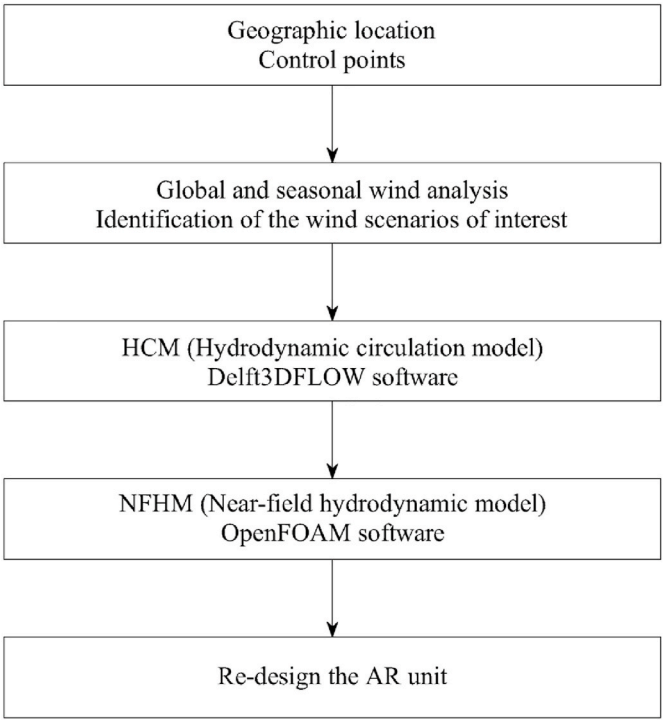

Fig. 3. Flowchart with the overall methodology applied.

close to the mouth of the Ría providing hourly wind data over a 18-year period (2006–2024) (Fig. 2). SIMAR dataset consists in numerically generated wind and wave data being available from 1958 and covering the North Atlantic, which is provided by the Spanish Port Authority (Puertos del Estado). In the case of wind data, they are generated by using different types of models, HIRLAM until 2018 which was substituted by and HARMONIE-AROME leading with to a higher spatial resolution and, over the last years also being extended to other regions such as the Mediterranean Sea, and port areas.

The resulting hydrodynamics in the zones and locations of interest provoked by the winds of interest are computed through a shallow water hydrodynamic circulation model (Delft3DFLOW), based on which velocity design parameters are defined. Finally, the velocity parameters obtained are used to re-design the site-specific AR configuration through a near-field hydrodynamic model (OpenFOAM). The work therefore aims to determine the effect of the wind-induced circulation which may lead to a modification in the existing AR design, and adapt it, if required, for the proper circulation near the cavities/nest, based on the consideration of velocity design parameters.

2.2. Numerical modelling of coastal hydrodynamics

As indicated in Fig. 3, the software Delft3DFLOW (Deltares, 2010) is used to investigate the 3D hydrodynamic characteristics of the Ría de Ares-Betanzos under upwelling events of different intensity, and to assess their capability to alter the average circulation in absence of winds. It consists in a state-of-the-art open-source model which approximates the Shallow Water equations under the Boussinesq assumption. As a result, it considers the continuity equation for an incompressible fluid (Eq. (1)), and the momentum equations which are simplified to the hydrostatic pressure distribution in its z-direction (Eq. (2)). In addition to the computation of barotropic flows resulting from the action of the tide, river discharges and wind, the model is also capable of assessing the baroclinic flows resulting from the complex interaction of the oceanic and riverine waters. To this end, Eq. (2) is coupled to the transport equation (Eq. (3)) as follows:

$$\frac{Du}{Dt} = fv - g\frac{\partial \zeta}{\partial x} - \frac{g}{\rho_0}\int_{z'=z}^{z'=\zeta}\frac{\partial \rho}{\partial x}dz' + \upsilon_h\left(\frac{\partial^2 u}{\partial x^2} + \frac{\partial^2 u}{\partial y^2}\right) + \upsilon_v\left(\frac{\partial^2 u}{\partial z^2}\right)\frac{Dv}{Dt} = -fu - g\frac{\partial \zeta}{\partial y} - \frac{g}{\rho_0}\int_{z'=z}^{z'=\zeta}\frac{\partial \rho}{\partial y}dz' + \upsilon_h\left(\frac{\partial^2 v}{\partial x^2} + \frac{\partial^2 v}{\partial y^2}\right) + \upsilon_v\left(\frac{\partial^2 v}{\partial z^2}\right)\frac{\partial p}{\partial z} = -\rho g \quad (2)$$

$$\frac{\partial u}{\partial x} + \frac{\partial v}{\partial y} + \frac{\partial w}{\partial z} = M \quad (1)$$

$$\frac{De}{Dt} = \kappa_h\left(\frac{\partial^2 e}{\partial x^2} + \frac{\partial^2 e}{\partial y^2}\right) + \kappa_v\frac{\partial^2 e}{\partial z^2} - d_e + E \quad (3)$$

in these equations *u, v* and *w* represent the velocity components of the flow in *x-, y-* and *z*-direction, respectively; ζ is the free surface water level; ρ_0 and ρ denote the reference density and density of ocean sea water, respectively; *M* is the source term of mass; *f* represents the Coriolis parameter; υ_h and υ_v account for turbulent eddy viscosity in horizontal and vertical directions, respectively; κ_h and κ_v account for the turbulent eddy diffusivity in horizontal and vertical directions, respectively; *e* denotes any constituent or element of interest, in the present application salinity and temperature; d_e stands for decay processes of 1st order of the constituent *e*; finally, *E* stands for the source of both salinity and temperature constituents.

For model application, a 100 m spatial resolution inside the Ría is considered. In addition, based on previous studies in the Galician Rías, and with the aim of appropriate modelling the influence of the offshore coastal area in the upwelling events inside the ria, the model extends up over the continental shelf increasing the grid size up to 250 m at over the continental shelf. The model also covers the adjacent Ría de A Coruña and Ría de Ferrol (Fig. 2), which may also influence the hydrodynamics of the Ría de Ares-Betanzos, primarily close to its mouth. Furthermore, when analysing upwelling events, the vertical discretization should consider an adequate number of layers to appropriately characterize the circulation throughout the whole water column. With this aim, a σ-grid model is applied, i.e., the layer size in *z*-direction is defined as a percentage of the water depth at each specific location, enabling a much better representation than other models, such as the *z*-grid model, in the case of the depth limited locations in the middle to inner Ría. Following previous works dealing with 3D complex flows in the Galician Rías (Iglesias and Carballo, 2009), a total number of 12 layers are considered with vertical size (%) of the total water depth from surface to bottom of: 2, 3, 5, 10, 15, 15, 15, 15, 10, 5, 3, 2.

With respect to the boundary conditions, at the open sea boundaries the water level is prescribed by imposing the tidal constituents as obtained from TOPEX/Poseidon database (Le Provost et al., 1995), along with average thermohaline conditions as provided by coastal buoys operated by Puertos del Estado covering large time periods close to the area of interest. In the inner Ría, river discharges are also imposed according to their corresponding gauging stations as provided by Xunta de Galicia (Regional Government). The boundary conditions at land margins were null flow through the boundary and zero shear stress (*free slip*). On the free surface, the wind stress exerted is modelled by:

$$\vec{\tau}_s = C_d\rho_a\left|\vec{U}_{10}\right|\vec{U}_{10}, \quad (4)$$

where $\vec{U}_{10}$ represents the wind velocity vector at a height of 10 m above the sea surface, ρ_a is the air density and C_d corresponds to a dimensionless drag coefficient, which is modelled according to Smith (1980) for wind velocities below 6 m s^{-1}, and following Yelland et al. (1998) for wind velocities above 6 m s^{-1}. Wind data is obtained from a SIMAR point in the area of study (Fig. 2) (see section 3 for further details on SIMAR dataset). At the bottom boundary, a quadratic stress law is prescribed (Deltares, 2010; Le Provost et al., 1995). Finally, the initial conditions are zero free surface elevation and velocity at all grid points (the so-called *cold start*). Thus, the model runs for a certain period before the period of interest to dynamically adjust the flow field and the thermohaline variables (*spin-up*).Prior to using the numerical model to characterize the hydrodynamics in the Ría de Ares-Betanzos under favourable wind upwelling conditions, its capability for accurately reproduce the hydrodynamics in this water body is demonstrated. With this aim, the model is calibrated and validated by comparing model results against field data of (i) water levels, and (ii) current velocity magnitude and direction at an intermediate depth, gathered by an Acoustic Doppler Current Profiler (ADCP) deployed in the middle Ría (Fig. 2) at a mean water depth of about 20 m. The measurements cover a total period of 23 days favourable to upwelling conditions (3–July 26, 2007) during which weak to high intensity winds were present, along with variable river discharges (please note that the discharge of River Mandeo into the Ría is regulated by a hydroelectric power plant. The wind field and river discharges present during the validation period and input to the model are plotted in Figs. 4 and 5, respectively.

To provide accurate results, the horizontal grid (spatial location) cell selected from the model corresponds to that closer to the ADCP. More specifically, the ADCP is located at X = 558717 m, Y = 4806047 m (UTM Zone 29) which corresponds with the model grid cell (m = 264, n = 131), whose centre is located at X = 558742 m, Y = 4806086 m (i.e., at 26 m distance).

In Fig. 6 the water levels as computed by the model (continuous line) and measured by the ADCP (dots) are provided. It is shown that the model can reproduce the water levels in the Ría with very high accuracy, as it is apparent by the virtually perfect overlapping between line and dots. This is corroborated by the resulting statistical parameters, with a

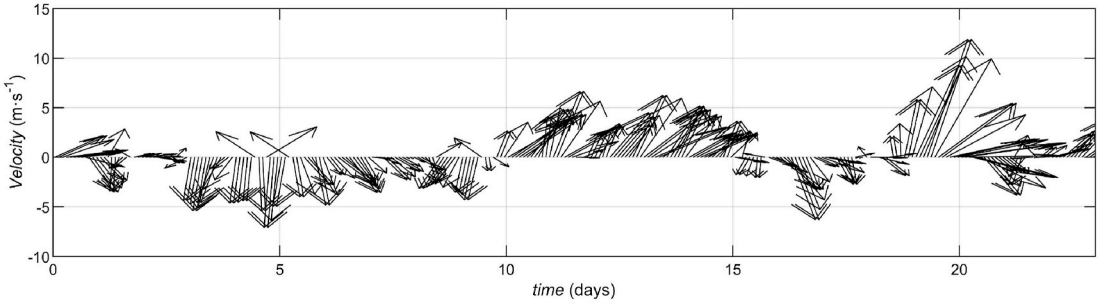

Fig. 4. – Hourly wind velocity and direction during the validation period (only one in two data is plotted for clarity).

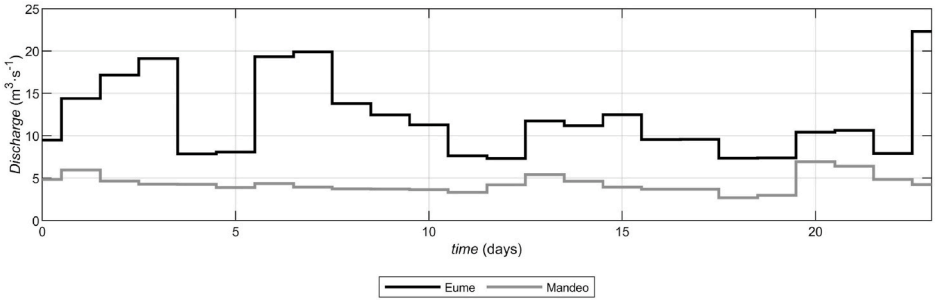

Fig. 5. – Daily river discharges flowing into the Ría de Ares-Betanzos (River Eume and River Mandeo) during the validation period.

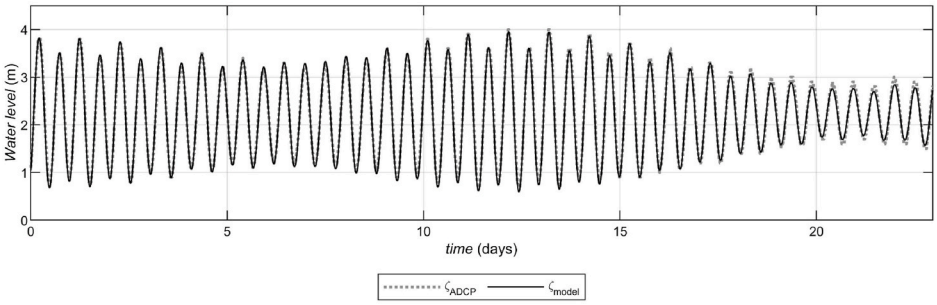

Fig. 6. – Water levels as computed by the model (continuous line) and measured by the ADCP (dots).

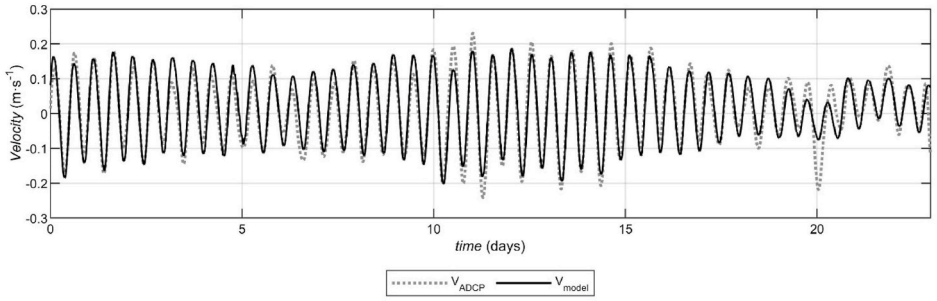

Fig. 7. – Current velocity component along the main ria axis computed by the model (continuous line) and measured by the ADCP (dots) at an intermediate water depth.

correlation coefficient, R, close to 1 ($R = 0.997$), and very low root mean square error, $RMSE = 0.0717$ m.

Next, in order to assess the capability of the model to reproduce the resulting circulation, the current velocity component in the main inflow-outflow direction is computed by projecting the velocity vector over an axis defining the main orientation of the estuary, which results in positive values indicating inflow and negative values outflow. This procedure has shown to be of high interest for hydrodynamic analysis in estuaries (Souto et al., 2003) insofar as the resulting velocities show flood and ebb periods along with their alteration by forcing factors different to the tide. Again, and in order to provide accurate results, the vertical grid cell (depth) selected from the model correspond to that closer to the ADCP. More specifically, the centre of the selected ADCP intermediate layer (that with less noise and inaccuracies) is located at 10.7 m of water depth, which corresponds with the vertical layer 7 located at 11.5 m of water depth. Fig. 7 shows the current velocity component along the main axis of the ria as computed by the model (continuous line) and measured by the ADCP (dots).

The results show the capability of the model to reproduce the hydrodynamics of this water body resulting not only by the tide, as it is

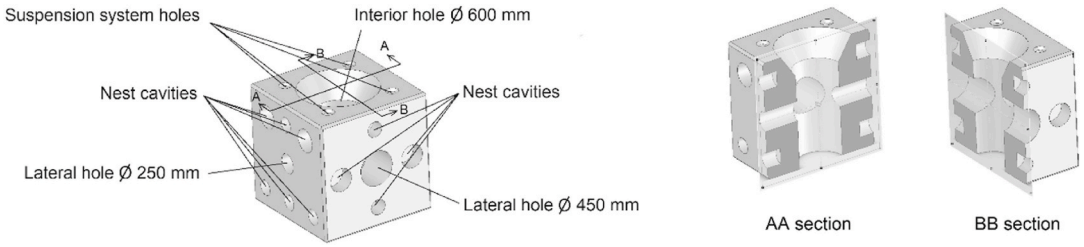

Fig. 8. – Artificial reef design.

shown by the accurate representation of flood and ebb flows, but also by the rest of the forcing factors. This is also apparent by the statistical fitting results obtained between model data and measurements, with a very high correlation coefficient, $R = 0.943$, and low root mean square error, $RMSE = 0.032$ m s^{-1}. The presence of a peak during the 20th day not captured by the model appears to be the result of malfunctioning or low frequency noise in the ADCP, insofar as during that day neither unusual strong winds (Fig. 4) or large river discharges (Fig. 5) were recorded.

2.3. AR design and modelling

The proposed ARs are shown in Fig. 8. This design was proposed in previous works (Carral et al., 2022; Lamas Galdo et al., 2022) according to biological, logistic, structural and hydrodynamic considerations corresponding to a complete spring-cycle under average circulation in absence of winds. In addition, ecological materials were proposed in the manufacturing process to produce "green" AR (Camba et al., 2021; Carral et al., 2023b). The faces present nest cavities of 200 mm and 300 mm in diameter, specifically designed for the species expected to colonize the AR. An inner hole of 600 mm in diameter connects the interior to the exterior, providing light and a pathway for nutrient uptake. In addition, two lateral holes of 250 mm and 450 mm in diameter, also connect the exterior to the interior. According to the conclusions of previous works (Carral et al., 2021), based on average current velocities in the Ría de Ares-Betanzos, it is more appropriate to orient the 250 mm diameter hole in the direction of the current(Carral et al., 2021).

For AR design, the OpenFOAM CFD software is used for the near-field hydrodynamic modelling. Like the Delft3DFLOW hydrodynamic circulation modelling, OpenFOAM is based on the continuity equation for an incompressible fluid (Eq. (1)), and the momentum equations. However, in this case, the near-field model is not simplified to the hydrostatic pressure distribution in its and z-direction since there is no large difference in vertical and horizontal length scales. Another difference is that the current velocity profile from the shallow water hydrodynamic circulation model is assumed to be stationary. Consequently, Eq. (5) is used as the momentum equation in the x, y and z directions.

$$\rho \frac{\partial}{\partial x_j}\left(u_i u_j\right) = -\frac{\partial p}{\partial x_i} + \frac{\partial \tau_{ij}}{\partial x_j} + \frac{\partial}{\partial x_j}\left(-\rho \overline{u_i' u_j'}\right) \tag{5}$$

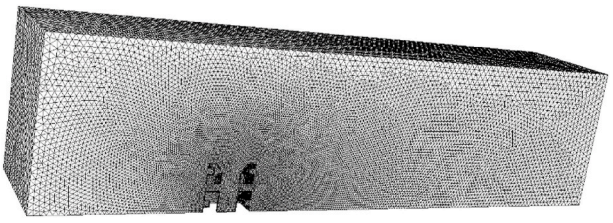

Fig. 9. – CFD computational grid.

in the equation above, τ_{ij} denotes the viscous stress tensor, while u_i and u_j represent the velocity components in the x, y, and z directions.

Regarding numerical parameters, OpenFOAM is based on the finite volume method. The RANS equations are solved together with the standard k-ε turbulence model. Water is treated as a Newtonian, incompressible, single-phase fluid. The pressure-velocity coupling is handled by the SIMPLE (Semi-Implicit Method for Pressure Linked Equations) algorithm. A second-order upwind scheme was used to discretize the governing equations.The domain consists of a cube with dimensions of 20,000 m, 5000 m and 4000 m, considered to be large enough to avoid boundary effects (Fig. 9). The grid size ranges from 0.005 m near the AR surfaces to 0.15 m on the outer surfaces. As can be seen, the AR is not centered within the computational domain, resulting in a larger rear section compared to the front. The main reason for this is to accurately capture the wake effects and turbulence generated by the AR. This setup allows the wake to develop and dissipate, along with ensuring realistic boundary conditions by preventing premature interaction with the outlet boundary, and providing space for the flow to recover to a natural state. On the other hand, the incoming flow in front of the AR varies its behaviour over a smaller region than the flow behind the AR.

For the boundary conditions, an inlet is applied on the left side of the domain, using the velocity profile from the Delft3DFLOW model, and an outlet on the right side of the domain. Non-slip boundary conditions are applied to both the AR surfaces and the seafloor. Due to symmetry, only half of the domain geometry is analysed.

The CFD model is validated based on previous experimental results (Carral et al., 2021; Santiago Caamaño et al., 2022);. In particular, the latter work (Santiago Caamaño et al., 2022) used results from tests carried out in the towed tank at the Ferrol campus (Universidad da Coruña) (Fig. 10). During these tests, the velocity field inside the AR was measured using a Nortek Vectrino velocimeter. In addition, two different orientations of the AR with respect to the current velocity were analysed: orientation A (with the 0.25 m diameter hole parallel to the current velocity), and orientation B (with the 0.45 m diameter hole parallel to the current velocity). The experimental results were compared with the numerical results obtained from CFD. Fig. 10 shows a comparison between the experimental and numerical velocities obtained at different points inside the artificial reef and corresponding to different current velocities. As can be seen, a satisfactory agreement was obtained, which confirms the validity of the CFD model for AR near-field modeling.

3. Metocean data analysis and upwelling favourable conditions

To investigate the wind conditions of interest in the Ría de Ares-Betanzos with capability to modify the average circulation in absence of winds, the closest set of large data currently available in the area, a SIMAR point located close to the Ría's mouth, is analysed. The dataset comprises hourly wind conditions during an 18-year period, from 2006 to 2024. In the present analysis, and for the sake of clarity, 45°

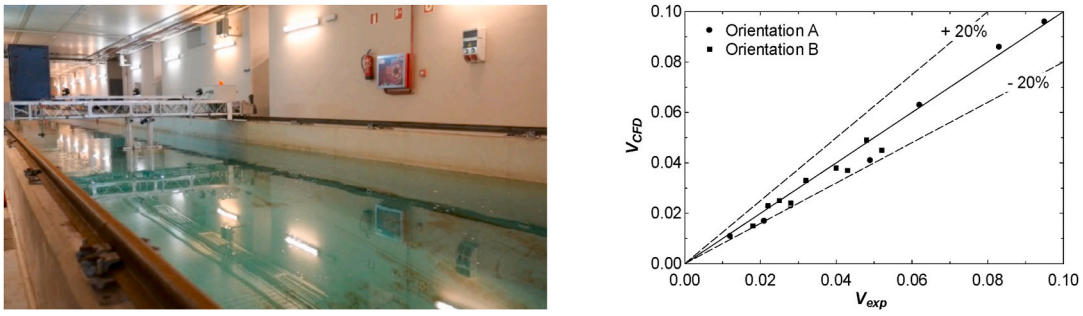

Fig. 10. – Facilities (towing tank) used for experimental tests (left); comparison between CFD and experimental results (right).

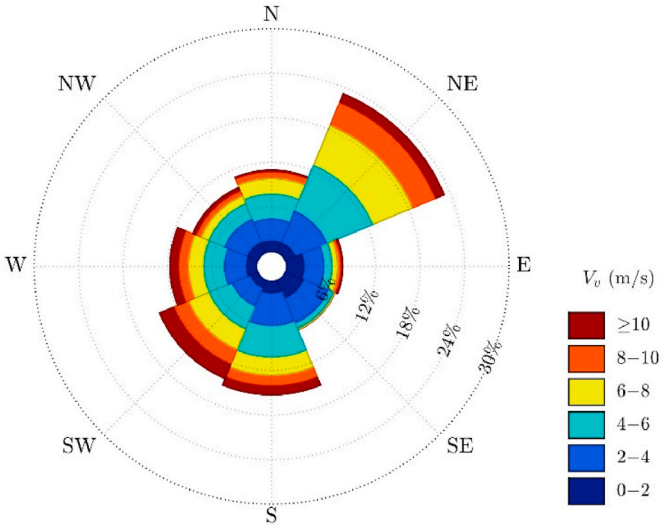

Fig. 11. – Global annual wind rose at SIMAR point.

directional sectors are retained.

A global annual analysis (Fig. 11) shows that the predominant wind directional sector is NE with and frequency of 23.18 % and average speed of 5.80 m s^{-1}, followed by S and SW attaining a similar occurrence with 15.29 % and 14.35 %, respectively, but with greater average speed in the case of the SW sector than S sector, with 6.43 m s^{-1} and 5.30 m s^{-1}, respectively. However, the identification of specific hydrodynamic events of interest taking place during given time periods, as it is the case of the circulation during upwelling wind favourable conditions —which is the aim of the present work—, based on global annual figures could lead to ill-informed conclusions; instead, intra-annual figures should be considered.

To this end, a seasonal analysis is also developed considering the following four time periods: Spring (March to May), Summer (June to August), Autumn (September to November), and Winter (December to February). The corresponding wind roses are plotted in Fig. 12.

During Spring and Summer, recognised as the most favourable period for upwelling in the Galician Rías, it is observed that the Ría de Ares-Betanzos is subject to northerly component winds, primarily from NE with similar figures during both seasons, with frequency, *f*, of 26.64 % and mean speed, V_m, of 5.99 m s^{-1} during Spring, and frequency of 28.24 % and mean speed of 5.87 m s^{-1} during Summer. In Autumn, and despite NE winds being also those with the largest occurrence leading to the presence of occasional upwelling events, southerly winds (S, SW and SE) present a similar joint occurrence (41.43 %) than northerly winds (NE, N, NW) (39.30 %). As Autumn progresses, the frequency and intensity of southerly winds increases, with S sector being during Winter that with the largest occurrence with 22.21 % and mean speed 5.90 m s^{-1}, followed by SW sector with 18.51 % but significantly greater wind velocity attaining 7.58 m s^{-1}. The aforementioned results are summarized in Table 1.

The identification of the most representative upwelling periods in the Galician Rías is complex. Probably, the most usual analysis resorts to a 6-month period including both Spring and Summer seasons (Carballo

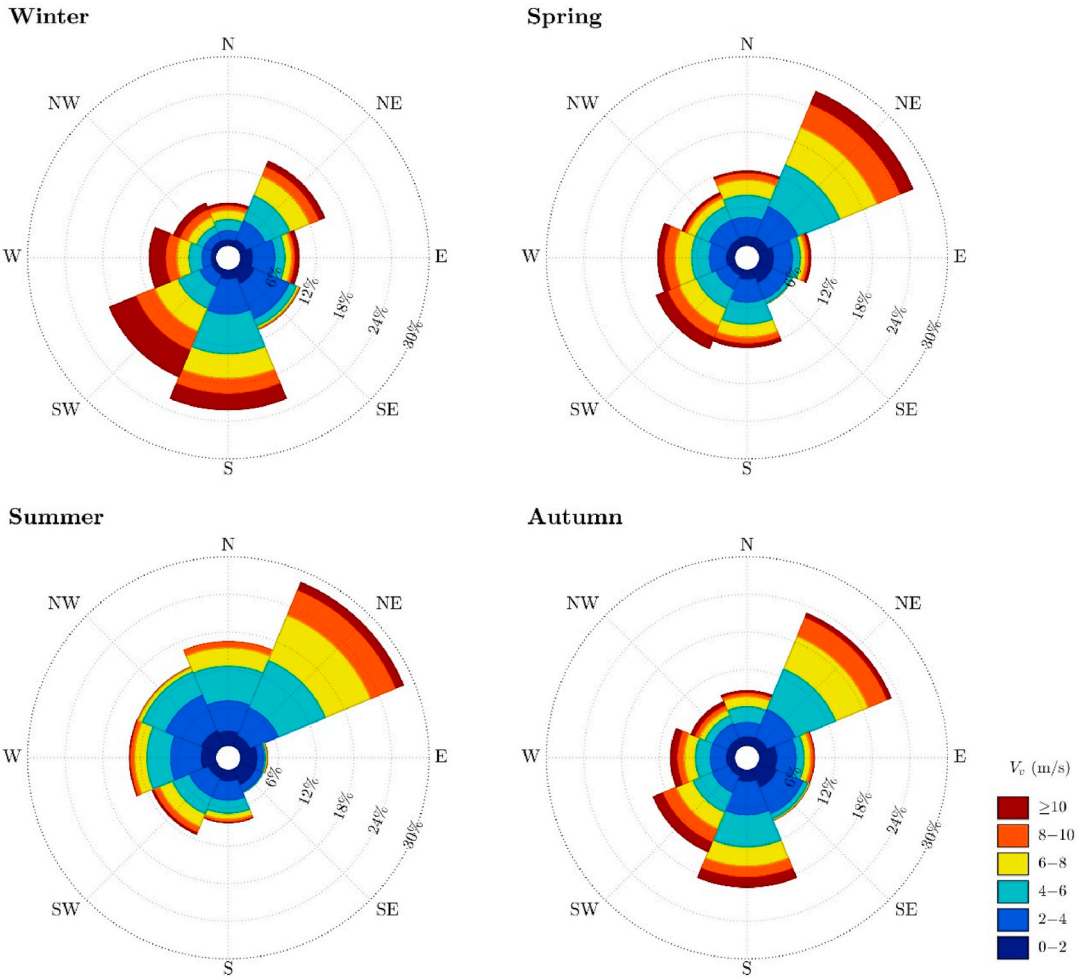

Fig. 12. Seasonal wind roses at SIMAR point.

Table 1
Wind scenarios retained for numerical modelling analysis. AUC: Average Upwelling Conditions; IUC: Intense Upwelling Conditions.

Season	*Direction*	*f* (%)	V_m (m s^{-1})	$V_{25\%}$ (m s^{-1})	$V_{m25\%}$ (m s^{-1})
Spring	NE	26.64	5.99	7.84	9.64
Summer	NE	28.24	5.87	7.60	9.03
Spring-Summer	NE	27.44	5.93 (AUC)	7.72	9.32 (IUC)

Table 2
Wind conditions and river discharges in numerical modelling case studies: AUC (Average Upwelling Conditions) and IUC (Intense Upwelling Conditions). For simplicity only river discharges within the Ría de Ares-Betanzos are indicated.

Conditions	*Wind Direction*	*Wind velocity* (m s^{-1})	Q_{Eume} (m^3 s^{-1})	Q_{Mandeo} (m^3 s^{-1})
AUC	NE	5.93	12.12	11.07
IUC	NE	9.32	12.12	11.97

et al., 2009). However, the consideration of other periods such as only Spring, and despite the almost negligible differences in the mean wind velocity with respect to Summer, may well lead to somewhat different hydrodynamic results, arising from the much larger river discharges during Spring than in Summer which tend to reinforce the NE wind induced circulation (Iglesias and Carballo, 2009).

Based on the above results and considerations, the following conditions are retained for its hydrodynamic analysis through numerical modelling, being representative of average conditions of wind-favourable upwelling, or AUC (Average Upwelling Conditions): Spring and Summer upwelling favourable conditions characterized by NE winds representing 27.44 % of time, and mean wind velocity of 5.93 m s^{-1} (Table 1), and the corresponding average river discharges flowing into this ria during the same period (Table 2).

With the aim of thoroughly analysing the capability of northerly winds to generate upwelling events, further scenarios may be also of interest. In this regard, upwelling under average wind conditions in the Rías Baixas is frequent, leading to a very high oceanic productivity. However, as stated, in the case of the Rías Altas the presence of ENACW (Easter North Atlantic Central Water) takes place easily on the shelf despite wind conditions being not very favourable, as it is the case of average wind velocities; nevertheless, these upwelling conditions need to present high intensity to substantially affect the middle and inner rias (Bode et al., 2005; Varela et al., 2001). Thus, the capability of average upwelling favourable winds to significantly modify the average circulation in the Ría de Ares-Betanzos in absence of winds is still to be established. A low or very low capability would imply that its action could be disregarded for AR design, and would require the consideration of winds of greater intensity as those of potential interest for AR design.

Previous research has not clearly established any specific threshold of wind velocity leading to intense upwelling events in this coastal region. According to previous studies in the Galician Rías, it can be

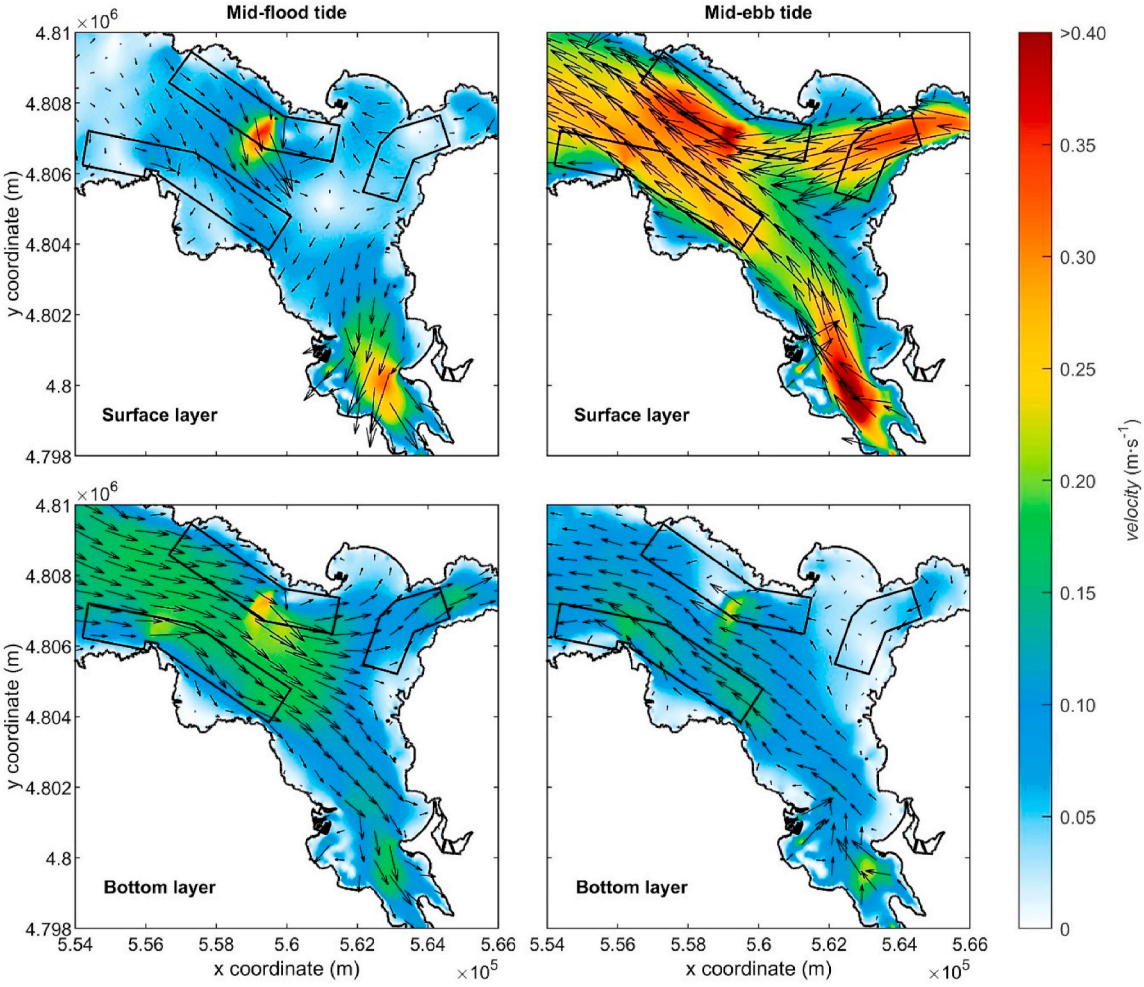

Fig. 13. – Average transient circulation during mid-flood (left) and mid-ebb tide (right) of a mean spring tide under average upwelling-favourable winds (AUC) at surface (above) and bottom (below) layers.

established that winds leading to intense upwelling events will be those coming from the upwelling favourable direction and with at least medium to high intensity blowing for a specific period of time. In this context, a wind velocity of 10 m s^{-1} identified as of "high winds" was used as that with the capability to generate intense upwelling (Iglesias and Carballo, 2010). Furthermore, this value has been also used as threshold for generating intense upwelling events in other coastal regions (Millot, 1979; Rahn and Garreaud, 2014).

It is important to note that the wind velocity resulting in intense upwelling should be defined considering their occurrence at each specific coastal region; in other words, to assume thresholds established for other coastal regions may lead to an underestimation of the duration of wind events leading to intense upwelling (Correa-Ramirez et al., 2020). Previous studies have analysed winds favourable to intense upwelling as those corresponding to the upper 25th percentile of wind velocity intensity (Aguirre et al., 2019). A wind analysis in the Ría de Ares-Betanzos shows that the mean wind velocity favourable to upwelling (NE directional sector) corresponding to the upper 25th percentile of velocity magnitude, $V_{m25\%}$, i.e., mean wind velocity over a time period with velocity magnitude exceeding $V_{25\%}$, meaning the threshold velocity exceeded over 25 % of the total time period considered, attain values of 9.63 m s^{-1} and 9.03 m s^{-1} for Spring and Summer, respectively, thereby being close to the 10 m s^{-1} figure previously used in the Galician Rías. Based on the results obtained, the aforementioned upper 25th percentile is retained in present work for further analysis. As in the case of average wind conditions, the consideration of the whole 6-month period is expected to be more representative for analysing the resulting wind-induced hydrodynamics.

Based on the above results and considerations, the following conditions are also retained for its hydrodynamic analysis through numerical modelling, representative of intense upwelling, or IUC (Intense Upwelling Conditions): Spring and Summer upwelling favourable conditions characterized by NE winds representing 27.44 % of time, and $V_{m25\%}$ equal to 9.32 m s^{-1} (Table 1), and the corresponding average river discharges flowing into this ria during the same period (Table 2).

4. 3D coastal hydrodynamics under upwelling events

After being validated, and once defined the case studies of interest, the shallow water model is applied to analyse the 3D average transient circulation in the Ría de Ares-Betanzos under wind-upwelling conditions (AUC and IUC) (Table 1) throughout a representative period. To this end, a complete average spring-neap tidal cycle under average river inflows and thermohaline conditions, with the presence of the aforementioned wind conditions, are considered, allowing comparison with previous studies (average river inflows and thermohaline conditions, in absence of winds) (Carral et al., 2023a).

In addition, the previous hydrodynamic studies for AR deployment were focused on the three zones (Z1, Z2 and Z3) (Fig. 2) identified as of interest considering an Integrated Coastal Zone Management (ICZM) approach (Carral et al., 2019). Their hydrodynamics were analysed by considering representative locations (L1, L2 and L3) (Fig. 2) through 2D numerical modelling (Carral et al., 2021), and 3D modelling in absence of winds (Carral et al., 2023a). These hydrodynamics results were used

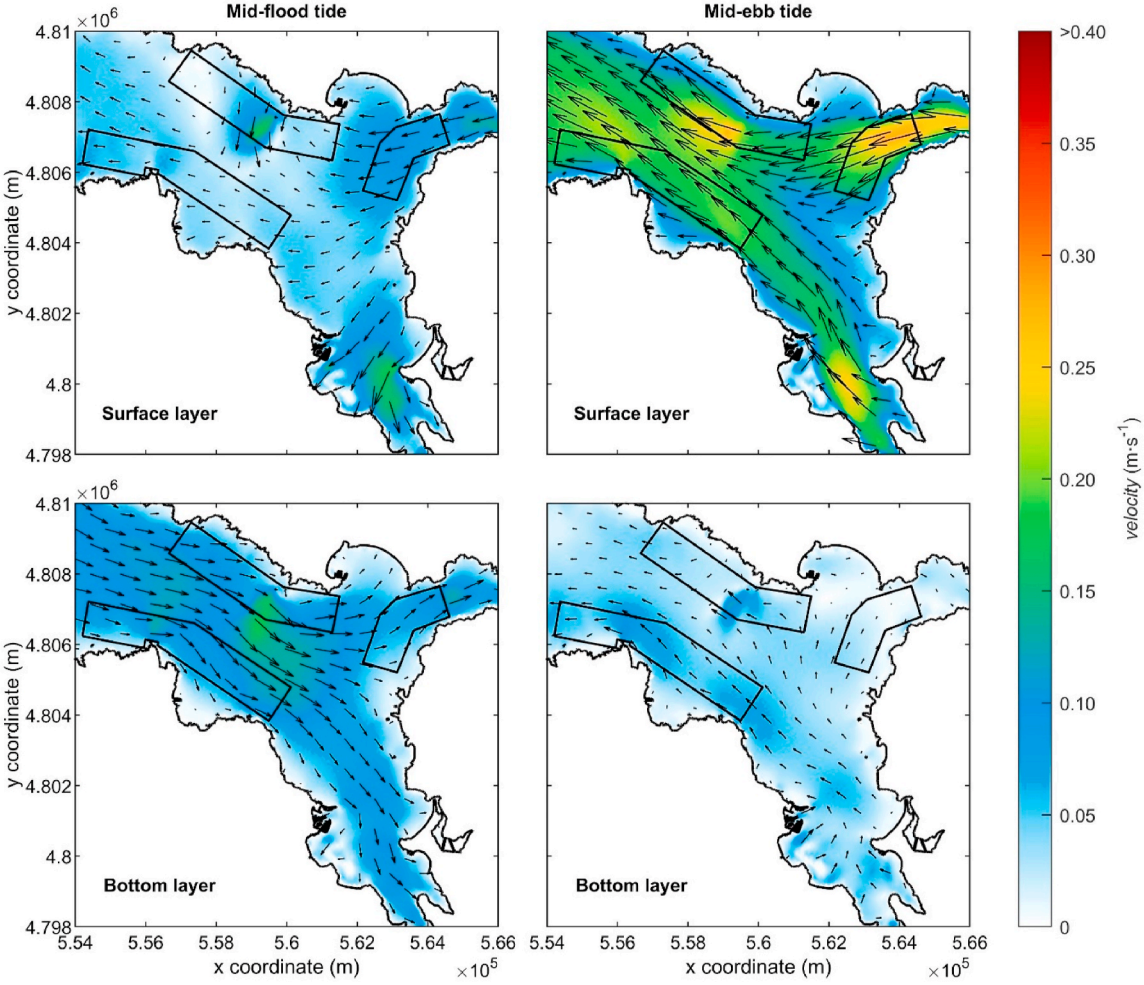

Fig. 14. – Average transient circulation during mid-flood (left) and mid-ebb tide (right) of a mean neap tide under average upwelling-favourable winds (AUC) at surface (above) and bottom (below) layers.

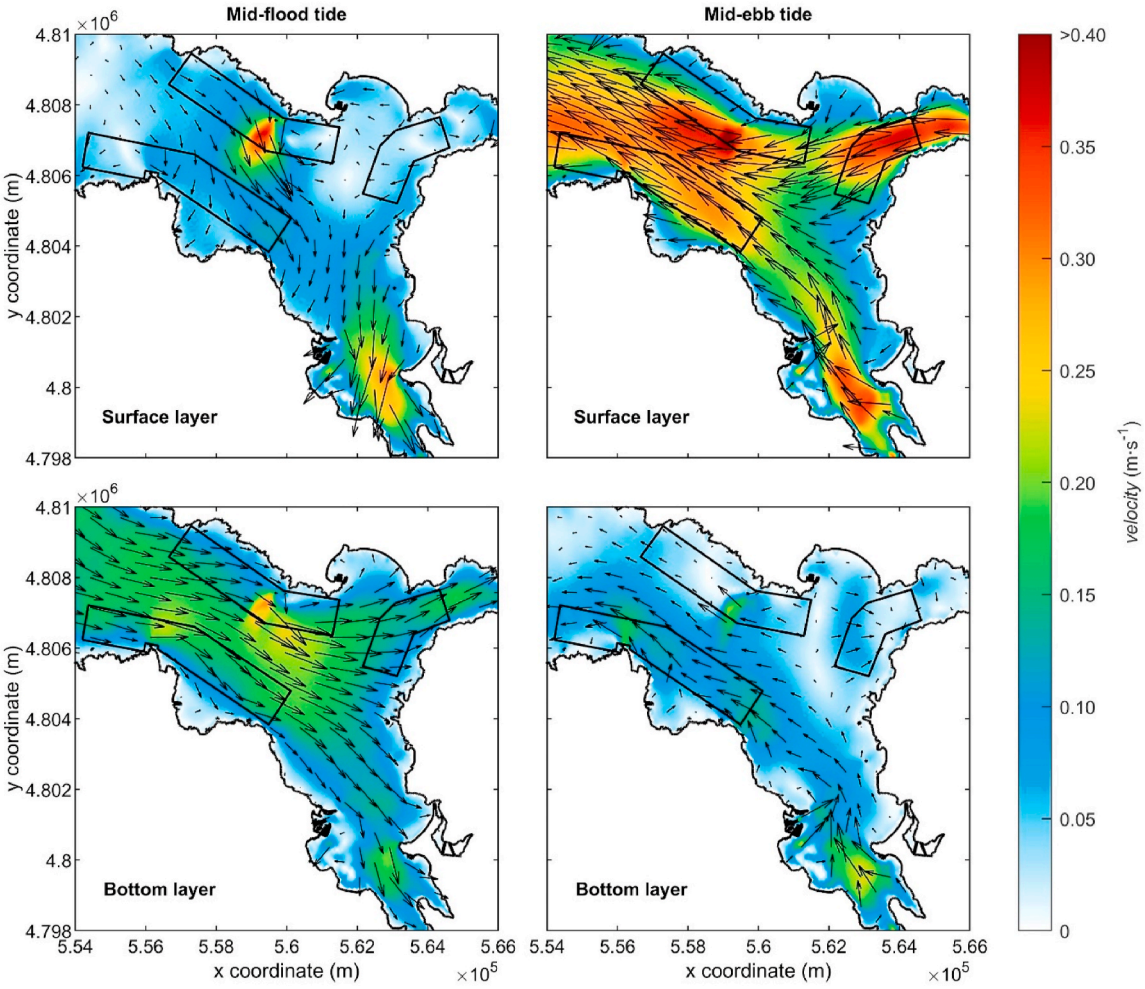

Fig. 15. – Average transient circulation during mid-flood (left) and mid-ebb tide (right) of a mean spring tide under average upwelling-favourable winds (IUC) at surface (above) and bottom (below) layers.

to define the best site-specific AR configurations. Thus, in order to analyse the influence of wind action on the definition of the AR configuration, the aforementioned zones and locations are also considered in the present work.

The resulting hydrodynamics during AUC at mid-flood and mid-ebb tide in surface and bottom layers are plotted for a mean spring (Fig. 13) and a mean neap tide (Fig. 14). It can be observed that the general hydrodynamics present similar patterns at both situations; however, there exist significant differences in the intensity of the currents. During mid-ebb tide at spring tides, large areas in Z2 and Z3 present current velocities greater than 0.30 m s^{-1}, exceeding 0.40 m s^{-1} at specific locations, with Z1 presenting somewhat weaker currents. During neap tides, the magnitude of the currents is significantly weaker, with extensive areas with about 0.25 m s^{-1}, in this case primarily in Z3 and to a lesser extent in Z2 and Z1, and peak velocities of about 0.30 m s^{-1}.

A comparison with the 3D hydrodynamics induced under average conditions in absence of winds (Carral et al., 2023a) shows that the general circulation patterns are not altered, which in turn correspond with a two-layer positive estuarine circulation, resulting from the barotropic flow induced by river discharges, which is reinforced by the presence of winds. This reinforcement leads to somewhat greater current velocities, being apparent as expected during mid-ebb tide in surface layers, while at other time points or vertical position, wind effects are virtually negligible. Finally, average winds virtually do not modify other flow patterns, as it is the case of the flow asymmetry, again presenting characteristics of greater complexity than 2DH patterns (Carral et al., 2021), with the magnitude of ebb flows being of greater magnitude than flood flows in surface layers. However, these differences are even greater in the presence of winds, insofar as the barotropic circulation induced by river inflows, which strengthen ebb tidal velocities and weaken flood velocities, is now reinforced by wind action. This flow pattern is balanced at bottom layers where an utterly different circulation develops, with the same overall characteristics as those presented in Carral et al. (2023a).

Overall, it can be stated that wind action in AUC is not capable of significantly altering the average circulation in absence of winds, generating upwelling conditions of limited intensity, which in turn, is coherent with previous research in the Rías Altas region. On this basis, and in order to assess the real capability of wind action to alter the average circulation in this Ría, IUC situation is also analysed. The resulting hydrodynamics during IUC at mid-flood and mid-ebb tide in surface and bottom layers are plotted for a mean spring (Fig. 15) and a mean neap tide (Fig. 16).

Despite the relatively high winds considered in IUC, the results shows that wind action is not capable of driving the circulation in this ria or significantly altering the average circulation, either considering the action of average upwelling favourable winds (Figs. 13 and 14), or even in absence of winds (Carral et al., 2023a). These results reinforce the conclusions of previous works stating the importance of river discharges in driving the circulation of this water body, and the need of high intensity winds to generate intense upwelling in the coastal shelf capable of introducing significant amounts of ENACW mass into the Rías Altas.

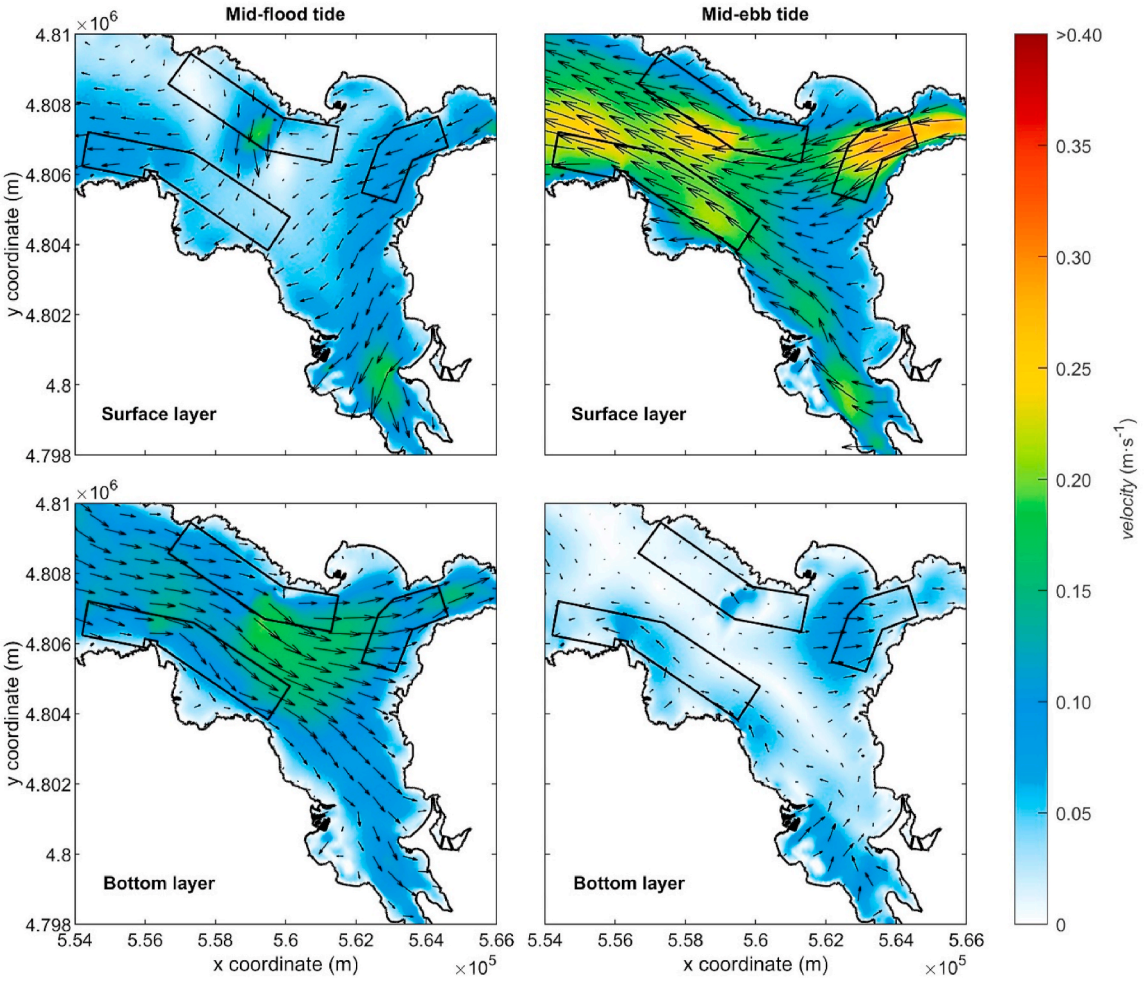

Fig. 16. – Average transient circulation during mid-flood (left) and mid-ebb tide (right) of a mean neap tide under average upwelling-favourable winds (IUC) at surface (above) and bottom (below) layers.

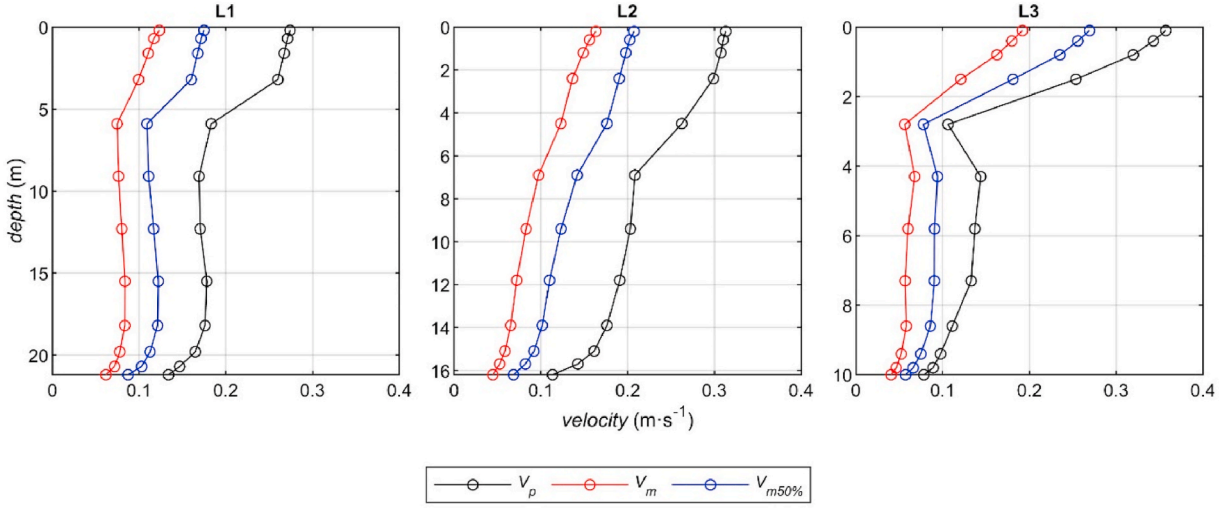

Fig. 17. – Results for the 3D site-specific velocity parameters at L1, L2 and L3 locations.

Based on the results obtained, it emerges that the importance of considering the wind action for AR design is limited. However, at specific locations, wind action may induce the sufficient hydrodynamic modification to, at least, be necessary to assess its influence in AR design process. In this regard, IUC situation presents a limited capability to significantly modifying the average circulation along with a low occurrence. Thus, it emerges that IUC presents less interest than AUC, with even lower overall capability to alter the circulation but with much larger occurrence (27.44 % during Spring-Summer). On this basis, AUC conditions are retained for analysis at the specific zones and locations of

interest L1, L2 and L3.

The site-specific analysis at these locations is conducted by computing its 3D flow structure throughout the water depth in terms of different velocity parameters identified as of interest for AR design based on hydrodynamic criteria (Carral et al., 2021): (i) V_p, which stands for the peak current velocity, (ii) V_m, representing the mean current velocity over the total period considered, and (iii) $V_{m50\%}$, being the mean current velocity over a period with the velocity magnitude exceeding $V_{50\%}$, or the threshold velocity exceeded over 50 % of the total period considered. In the present application, a complete average spring-neap tidal cycle is considered. (Fig. 17).

From a detailed analysis of the velocity vertical profiles, which

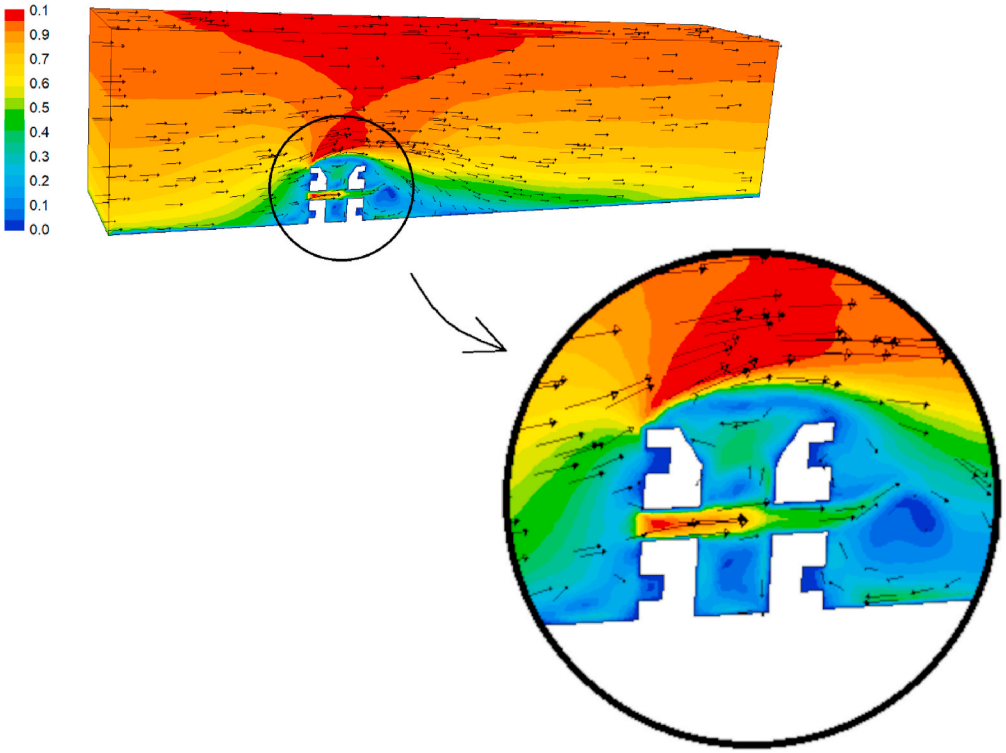

Fig. 18. – Velocity field (m s^{-1}) around the AR. L3 location under $V_{m50\%}$ conditions. 250 mm lateral hole.

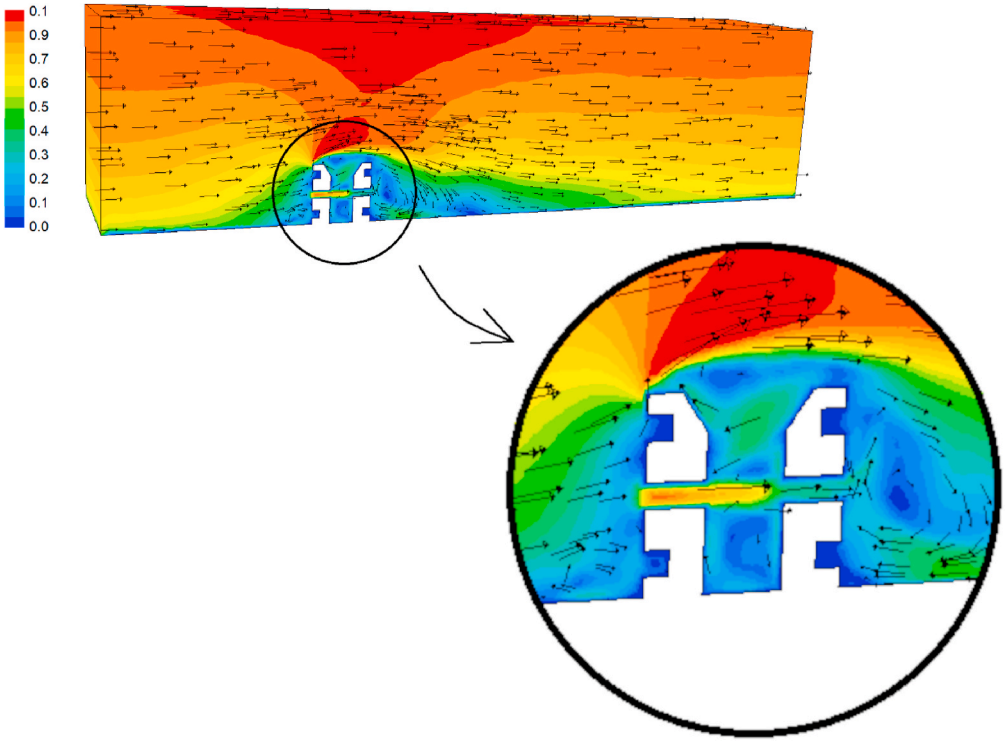

Fig. 19. – Velocity field (m s^{-1}) around the AR. L3 location under $V_{m50\%}$ conditions. 200 mm lateral hole.

confirm the previous results of general flow patterns in surface and bottom layers, further information of interest can be found. It is observed that whereas L1 and L2 presents similar results to those in the absence of winds, flow velocities at L3, in particular at a representative water depth for AR operation (layer 10) are significant altered, with V_p, V_m and $V_{m50\%}$ attaining 0.097 m s^{-1}, 0.052 m s^{-1} and 0.075 m s^{-1}, respectively, showing an increase of about 12 %, 30 % and 27 %, respectively. This can be the result of Z3 being located in the inner Ría, in a branch with its main axis being roughly aligned with NE winds, along with limited water depth (about 10 m), and thus subject to significant effects in the resulting circulation under upwelling-favourable winds.

Thus, and on the basis of these results, it can be established that wind action can be neglected for AR design at L1 and L2; however, its influence at L3 requires further assessment through CFD modelling (Section 5).

5. Adaptation of AR design to upwelling events

In the present work the velocity parameter corresponding to $V_{m50\%}$ under average upwelling conditions (AUC) is retained for AR design. The resulting velocity near-field provided by the CFD hydrodynamic model for flow behaviour prediction at L3 is shown in Fig. 18. This figure corresponds to the design previously shown in Fig. 8, with a 250 mm diameter hole oriented in the direction of the current. As observed, the AR modifies the velocity field and, considering that POM disperses along the water flow (Kim et al., 2024), enhances circulation. Two significant vortices are generated. One of them is due to the water current that separates from the seafloor and moves upward. This vortex is essential to promote vertical water circulation, which could potentially increase nutrient circulation transport from the seafloor. The other vortex forms behind the AR. This vortex is critical for promoting circulation in the area sheltered from the current velocity.

The velocity field shown in Fig. 18 indicates that the selected AR design is adequate for providing water renewal. However, a diameter of the central hole smaller than 250 mm is sufficient to ensure an appropriate water flow. The effect of reducing the size of this lateral hole is analysed for current velocities obtained during average upwelling conditions, since high current velocities ensure circulation to the AR even with a smaller entrance hole. The results corresponding to the 200 mm hole are shown in Fig. 19. As can be seen in this figure, the 200 mm lateral diameter is more appropriate for these conditions. This size is sufficient to ensure proper water circulation into the interior of the AR while maintaining the top and back vortices that are also essential for circulation to the outer surfaces of the AR. At the same time, this solution does not reach such high speeds in the interior of the reef, providing a more comfortable environment for the resident species in the interior.

6. Conclusions

The design of AR should be adapted to the site-specific hydrodynamic characteristics of the coastal area of interest, which results from the influence that the water circulation has on the production of coastal ecosystems. Despite the currents in estuaries being driven primarily by the tide, river discharges and its mixing with oceanic waters, wind action may play also an important role, in particular during specific situations, such as upwelling wind-favourable conditions. This study addresses the importance of considering the wind-induced circulation for AR site-specific design in estuaries, being illustrated for a coastal area of great interest for AR deployment, the Ría de Ares-Betanzos, a specific type of estuary in the NW Iberian Peninsula. To this end, the wind conditions with the capability of modifying the average circulation in absence of winds are thoroughly analysed. More specifically, a global and seasonal wind analysis is developed to identify the wind scenarios of interest, in particular winds generating both average upwelling and intense upwelling. Then, a shallow water hydrodynamic circulation model is applied to characterize the coastal hydrodynamics under the obtained wind conditions. The influence of wind-induced hydrodynamics on the design of a reef unit is further investigated by developing CFD model for near-field hydrodynamic analysis around the AR by using as input the conditions obtained from the shallow water model. It is found that the capability of wind action to alter the average circulation in absence of winds, and thus to require the adaptation of the design of the AR is limited. However, at certain locations, wind action may induce sufficient hydrodynamic changes so that certain adaptation in the design may be appropriate. Considering average upwelling conditions —those shown as of higher interest for AR design—, an adaptation of the design at a specific location obtained for average conditions in absence of winds is proposed, consisting in the reduction of the size of a lateral hole that connects the outside with the inside of the reef.

CRediT authorship contribution statement

Rodrigo Carballo: Writing – original draft, Supervision, Methodology, Investigation, Conceptualization. **Iván López:** Writing – review & editing, Visualization, Investigation, Formal analysis, Conceptualization. **David Mateo Fouz:** Visualization, Validation, Resources, Investigation, Formal analysis. **María Isabel Lamas:** Writing – original draft, Validation, Methodology, Investigation, Conceptualization. **Luis Carral:** Writing – review & editing, Supervision, Methodology, Funding acquisition, Conceptualization.

Declaration of competing interest

The authors declare that they have no known competing financial interests or personal relationships that could have appeared to influence the work reported in this paper.

Acknowledgements

This research was funded by Xunta de Galicia under the grant CN-10MMA003CT. This study was also funded through the collaboration agreement INV07520 between Xunta de Galicia, Universidade da Coruña, and the Universidade da Coruña Foundation (FUAC) to give continuity to the previous project.

Data availability

Data will be made available on request.

References

Aguirre, C., Rojas, M., Garreaud, R.D., Rahn, D.A., 2019. Role of synoptic activity on projected changes in upwelling-favourable winds at the ocean's eastern boundaries. Npj. Clim. Atmos. Sci. 2 (1), 44. https://doi.org/10.1038/s41612-019-0101-9.

Bacher, C., Grant, J., Hawkins, A.J.S., Fang, J., Zhu, M., Besnard, M., 2003. Modelling the effect of food depletion on scallop growth in Sungo Bay (China). Aquat. Living Resour. 16 (1), 10–24. https://doi.org/10.1016/S0990-7440(03)00003-2.

Bode, A., González, N., Rodríguez, C., Varela, M., Varela, M.M., 2005. Seasonal variability of plankton blooms in the Ria de Ferrol (NW Spain): I. Nutrient concentrations and nitrogen uptake rates. Estuar. Coast Shelf Sci. 63 (1), 269–284. https://doi.org/10.1016/j.ecss.2004.11.020.

Bohnsack, J.A., Sutherland, D.L., 1985. Artificial reef research: a review with recommendations for future priorities. Bull. Mar. Sci. 37 (1), 11–39.

Bracho-Villavicencio, C., Matthews-Cascon, H., García-Durán, M., Vélez, X., Lago, N., Busquier, L., Rossi, S., 2024. Benthic colonization on new materials for marine ecosystem restoration in porto cesareo, Italy. J. Mar. Sci. Eng. 12 (1). https://doi.org/10.3390/jmse12010169.

Camba, C., Mier, J.L., Carral, L., Lamas, M.I., Álvarez, J.C., Díaz-Díaz, A., Tarrío-Saavedra, J., 2021. Erosive degradation study of concrete augmented by mussel shells for marine construction. J. Mar. Sci. Eng. 9 (10). https://doi.org/10.3390/jmse9101087.

Carballo, R., Iglesias, G., Castro, A., 2009. Residual circulation in the Ría de Muros (NW Spain): A 3D numerical model study. J. Mar. Syst. 75 (1–2), 130.

Carral, L., Alvarez-Feal, C., Jesús Rodríguez-Guerreiro, M., Vargas, A., Arean, N., Carballo, R., 2019. Methodology for positioning a group of green artificial reef based on a database management system, applied in the estuary of Ares-Betanzos (Nw

Iberian Peninsula). J. Clean. Prod. 233, 1047–1060. https://doi.org/10.1016/j.jclepro.2019.06.092.
Carral, L., Lamas–Galdo, M.I., Rodríguez-Guerreiro, M.J., Vargas, A., Álvarez-Feal, C., López, I., Carballo, R., 2021. Configuration methodology for a green variety reef system (AR group) based on hydrodynamic criteria – Application to the Ría de Ares-Betanzos. Estuar. Coast Shelf Sci. 252, 107301. https://doi.org/10.1016/j.ecss.2021.107301.
Carral, L., Lamas, M.I., Cartelle Barros, J.J., López, I., Carballo, R., 2022. Proposed conceptual framework to design artificial reefs based on particular ecosystem ecology traits. Biology 11 (5). https://doi.org/10.3390/biology11050680.
Carral, L., Lamas, M.I., Fouz, M., López, I., Carballo, R., 2023a. Improvements in the design of nest cavities to attract cephalopods and crustaceans in a green artificial reef unit according to tridimensional hydrodynamic criteria – application to the Ares-Betanzos estuary. Ocean Coast Manag. 245, 106871. https://doi.org/10.1016/j.ocecoaman.2023.106871.
Carral, L., Lamas-Galdo, M.I., Buenhombre, J.L.M., Barros, J.J.C., Naya, S., Tarrio-Saavedra, J., 2023b. Application of residuals from purification of bivalve molluscs in Galician to facilitate marine ecosystem resiliency through artificial reefs with shells – one generation. Sci. Total Environ. 856, 159095. https://doi.org/10.1016/j.scitotenv.2022.159095.
Correa-Ramirez, M., Rodriguez-Santana, Á., Ricaurte-Villota, C., Paramo, J., 2020. The Southern Caribbean upwelling system off Colombia: water masses and mixing processes. Deep Sea Res. Oceanogr. Res. Pap. 155, 103145. https://doi.org/10.1016/j.dsr.2019.103145.
David da Costa, I., Luís da Silva Santos, J., Costa, L.L., Lima, J.S., Zalmon, I.R., 2022. Reproductive potential and production role of artificial reefs - southeastern Brazil. Estuar. Coast Shelf Sci. 265, 107710. https://doi.org/10.1016/j.ecss.2021.107710.
Deltares, 2010. User Manual Delft3D-FLOW, Deltares ed.
Duarte, P., Alvarez-Salgado, X.A., Fernández-Reiriz, M.J., Piedracoba, S., Labarta, U., 2014. A modeling study on the hydrodynamics of a coastal embayment occupied by mussel farms (Ria de Ares-Betanzos, NW Iberian Peninsula). https://doi.org/10.1016/j.ecss.2014.05.021.
Falcão, M., Santos, M.N., Drago, T., Serpa, D., Monteiro, C., 2009. Effect of artificial reefs (southern Portugal) on sediment–water transport of nutrients: importance of the hydrodynamic regime. Estuar. Coast Shelf Sci. 83 (4), 451–459. https://doi.org/10.1016/j.ecss.2009.04.028.
Feng, J., Zhao, X., Bi, F., Zhao, W., Zhao, L., Song, H., Yang, M., Hu, Z., Zhou, C., Shi, P., Hu, P., Ma, P., Sun, P., Jiang, H., Xu, J., Zhang, T., 2023. Investigating food web structure and system function of an artificial reef ecosystem based on carbon and nitrogen stable isotope analysis: implications for reef management. Front. Mar. Sci. 10.
González-Garcés Santiso, A., Vilas, F., Álvarez Salgado, X.A., 2008. La Ría de Vigo : una aproximación integral al ecosistema marino de la Ría de Vigo. Instituto de Estudios Vigueses.
Han, A., Yang, J.T., Chen, M., Zheng, Z., Yin, X., Lin, H., Xu, M.N., Kao, S., 2024. Hydrological connectivity controls on the dynamics of particulate organic matter in a semi-enclosed mariculture bay. Aquaculture 578, 740109. https://doi.org/10.1016/j.aquaculture.2023.740109.
Iglesias, G., Carballo, R., 2009. Seasonality of the circulation in the Ría de Muros (NW Spain). J. Mar. Syst. 78 (1), 94–108. https://doi.org/10.1016/j.jmarsys.2009.04.002.
Iglesias, G., Carballo, R., 2010. Effects of high winds on the circulation of the using a mixed open boundary condition: the Ría de Muros, Spain. Environ. Model. Software 25 (4), 455–466. https://doi.org/10.1016/j.envsoft.2009.10.013.
Kim, D., Jeong, J., Jung, S., Na, W., 2024. Evaluating the particulate organic matter particles distribution characteristics around artificial reefs using computational fluid dynamics. Ocean. Eng. 292, 116574. https://doi.org/10.1016/j.oceaneng.2023.116574.
Lamas Galdo, M.I., Rodríguez Guerreiro, M.J., Lamas Vigo, J., Ameneiros Rodriguez, I., Veira Lorenzo, R., Carral Couce, J.C., Carral Couce, L., 2022. Definition of an artificial reef unit through hydrodynamic and structural (CFD and FEM) models—application to the ares-betanzos estuary. J. Mar. Sci. Eng. 10 (2). https://doi.org/10.3390/jmse10020230.
Le Provost, C., Bennett, A.F., Cartwright, D.E., 1995. Ocean tides for and from topex/poseidon. Science 267 (5198), 639–647.
Libes, S., 2011. Introduction to Marine Biogeochemistry. Academic Press.
Lima, J.S., Sanchez-Jerez, P., dos Santos, L.N., Zalmon, I.R., 2020. Could artificial reefs increase access to estuarine fishery resources? Insights from a long-term assessment. Estuar. Coast Shelf Sci. 242, 106858. https://doi.org/10.1016/j.ecss.2020.106858.
Millot, C., 1979. Wind induced upwellings in the gulf of lions. Oceanol. Acta 2 (3), 261–274.
Na, W., 2023. Artificial reefs research. J. Mar. Sci. Eng. 11 (1). https://doi.org/10.3390/jmse11010166.
Portugal, A.B., Carvalho, F.L., de Macedo Carneiro, P.B., Rossi, S., de Oliveira Soares, M., 2016. Increased anthropogenic pressure decreases species richness in tropical intertidal reefs. Mar. Environ. Res. 120, 44–54. https://doi.org/10.1016/j.marenvres.2016.07.005.
Rahn, D.A., Garreaud, R.D., 2014. A synoptic climatology of the near-surface wind along the west coast of South America. Int. J. Climatol. 34 (3), 780–792. https://doi.org/10.1002/joc.3724.
Ramos-Esplá, A.A., Guillén, J.E., Bayle, J.T., Sánchez-Jérez, P., 2000. Artificial anti-trawling reefs off alicante, south- eastern iberian Peninsula: evolution of reef block and set designs. In: Jensen, A.C., Collins, K.J., Lockwood, A.P.M. (Eds.), Artificial Reefs in European Seas. Springer, Netherlands, pp. 195–218. https://doi.org/10.1007/978-94-011-4215-1_12.
Reis, B., van der Linden, P., Pinto, I.S., Almada, E., Borges, M.T., Hall, A.E., Stafford, R., Herbert, R.J.H., Lobo-Arteaga, J., Gaudêncio, M.J., Tuaty-Guerra, M., Ly, O., Georges, V., Audo, M., Sebaibi, N., Boutouil, M., Blanco-Fernandez, E., Franco, J.N., 2021. Artificial reefs in the North –East Atlantic area: present situation, knowledge gaps and future perspectives. Ocean Coast Manag. 213, 105854. https://doi.org/10.1016/j.ocecoaman.2021.105854.
Sánchez-Caballero, C.A., Borges-Souza, J.M., Chavez-Hidalgo, A., Abelson, A., 2023. Assessing benthic reef assemblages: a comparison between no-take artificial reefs and partially protected natural reefs. Estuar. Coast Shelf Sci. 287, 108347. https://doi.org/10.1016/j.ecss.2023.108347.
Santiago Caamaño, L., Lamas Galdo, M.I., Carballo, R., López, I., Cartelle Barros, J.J., Carral, L., 2022. Numerical and experimental analysis of the velocity field inside an artificial reef. Application to the ares-betanzos estuary. J. Mar. Sci. Eng. 10 (12). https://doi.org/10.3390/jmse10121827.
Smith, S.D., 1980. Wind stress and heat flux over the ocean in gale force winds. J. Phys. Oceanogr. 10 (5), 709–726. May 1980.
Souto, C., Gilcoto, M., Fariña-Busto, L., Pérez, F.F., 2003. Modeling the residual circulation of a coastal embayment affected by wind-driven upwelling: Circulation of the Ría de Vigo (NW Spain). J. Geophys. Res. 108 (C11), 4–18.
Swarzenski, P.W., Campbell, P.L., Osterman, L.E., Poore, R.Z., 2008. A 1000-year sediment record of recurring hypoxia off the Mississippi River: the potential role of terrestrially-derived organic matter inputs. Mar. Chem. 109 (1), 130–142. https://doi.org/10.1016/j.marchem.2008.01.003.
Varela, M., Prego, R., Belzunce, M.J., Salas, F.M., 2001. Inshore–offshore differences in seasonal variations of phytoplankton assemblages: the case of a Galician Ria Alta (Ria de A Coruña) and its adjacent shelf (NW of Spain). Cont. Shelf Res. 21 (16), 1815–1838. https://doi.org/10.1016/S0278-4343(01)00032-2.
Wang, G., Wan, R., Wang, X., Zhao, F., Lan, X., Cheng, H., Tang, W., Guan, Q., 2018. Study on the influence of cut-opening ratio, cut-opening shape, and cut-opening number on the flow field of a cubic artificial reef. Ocean. Eng. 162, 341–352. https://doi.org/10.1016/j.oceaneng.2018.05.007.
Wilking, L.E., Dillon, K.S., Rakocinski, C.F., 2023. Artificial reef biofouling community impacts on ecosystem metabolism and biogeochemical cycling in estuarine waters of the northern Gulf of Mexico. Estuar. Coast Shelf Sci. 295, 108555. https://doi.org/10.1016/j.ecss.2023.108555.
Xu, Q., Zhang, L., Zhang, T., Zhang, X., Yang, H., 2017. Functional groupings and food web of an artificial reef used for sea cucumber aquaculture in northern China. J. Sea Res. 119, 1–7. https://doi.org/10.1016/j.seares.2016.10.005.
Xue, D., Wang, C., Huang, T., Pan, Y., Zhang, N., Zhang, L., 2023. Flow field effects and physical stability of pyramidal artificial reef with different slope angles. Ocean. Eng. 283, 115059. https://doi.org/10.1016/j.oceaneng.2023.115059.
Yelland, M.J., Moat, B.I., Taylor, P.K., Pascal, R.W., Hutchings, J., Cornell, V.C., 1998. Wind stress measurements from the open ocean corrected for airflow distortion by the ship. J. Phys. Oceanogr. 28 (7), 1511–1526.
Zhang, R., Zhang, H., Liu, H., Zhao, J., 2021. Differences in trophic structure and trophic pathways between artificial reef and natural reef ecosystems along the coast of the North yellow Sea, China, based on stable isotope analyses. Ecol. Indic. 125, 107476. https://doi.org/10.1016/j.ecolind.2021.107476.
Zhang, Z., Wang, M., Song, J., Zhao, W., Yu, D., Tang, X., Zhang, X., Liu, H., 2020. Food web structure prior to and following construction of artificial reefs, based on stable isotope analysis. Regional. Stud. Marine. Sci. 37, 101354. https://doi.org/10.1016/j.rsma.2020.101354.
Zhu, Z., Zhang, J., Wu, Y., Zhang, Y., Lin, J., Liu, S., 2011. Hypoxia off the changjiang (yangtze river) estuary: oxygen depletion and organic matter decomposition. Mar. Chem. 125 (1), 108–116. https://doi.org/10.1016/j.marchem.2011.03.005.